Available online at www.sciencedirect.com
ScienceDirect
Journal of Sound and Vibration 322 (2009) 167–183
JOURNAL OF SOUND AND VIBRATION
www.elsevier.com/locate/jsvi

A wave propagation and vibration-based approach for damage identification in structural components

Sauvik Banerjee[a,*], Fabrizio Ricci[b], Ernesto Monaco[b], Ajit Mal[c,1]

[a]*Department of Civil Engineering, Indian institute of technology-Bombay, Powai, Mumbai 400076, India*
[b]*Department of Aerospace Engineering, University of Naples Federico II, Via Claudio 21, 80125 Naples, Italy*
[c]*Mechanical and Aerospace Engineering Department, University of California, Los Angeles, CA 90095-1597, USA*

Received 30 August 2007; received in revised form 19 October 2008; accepted 7 November 2008
Handling Editor: S. Bolton
Available online 31 December 2008

Abstract

A damage index (DI) approach for damage detection and localization based on high frequency wave propagation data and low frequency vibration measurements is presented. Improved ultrasonic and vibration test setups, consisting of either distributed high-fidelity piezoelectric sensor arrays or laser vibrometer, data acquisition boards, signal conditioning and dedicated software have been implemented. In the wave propagation measurements, the data consist of broadband signals due to ultrasonic waves propagating in the structure, while in the vibration measurements they are modal response of the structure produced by the actuators. Using the initial measurements performed on an undamaged structure as baseline, damage indices are evaluated from the comparison of the frequency response of the monitored structure with an unknown damage. In case of wave propagation measurements, a damaged/undamaged path mechanism is used to approximately locate the damage using the correlations obtained between the statistical DI (statistic t) values at the sensor locations (control points). For vibration measurements, both piezoelectric patches and the laser vibrometer are used as response sensors in an effort to examine their sensitivity to damage detection. It is found that the laser vibrometer acquisitions produce improved sensitivity and higher accuracy of the DI when compared to piezo-patches as response sensors. In addition, Modal Assurance Criterion (MAC) has been used to compare and quantify the changes in the modal parameters evaluated from the measurements carried out on the healthy and damaged structure. The DI approach is used to identify various types of defects in the form of loose rivet holes, delaminations due to low velocity impact and added mass for changes in the stiffness, in both metallic and composite structural components with relatively complex geometries. It is shown that the procedure is able to identify an emerging and/or growing defect, with some degree of confidence.

*Corresponding author. Tel.: +91 22 2576 7343 (O), +91 22 2576 8343 (R), +91 9930679245 (mobile); fax: +91 22 2576 7302.
E-mail addresses: sauvik@civil.iitb.ac.in, sauvikbanerjee@gmail.com (S. Banerjee), fabricci@unina.it (F. Ricci), ermonaco@unina.it (E. Monaco), ajit@ucla.edu (A. Mal).
URL: http://www.civil.iitb.ac.in/~sauvik (S. Banerjee).
[1]Tel.: +1 310 825 5481; fax: +1 310 206 4830.

0022-460X/$ - see front matter © 2008 Elsevier Ltd. All rights reserved.
doi:10.1016/j.jsv.2008.11.010

1. Introduction

Much of structural health monitoring research is motivated by the fact that damage tolerant and fail-safe design of aircraft, aerospace and civil structures requires a substantial amount of inspection and defects-monitoring at regular intervals [1–3]. With the risk of failure and the cost of scheduled but unneeded maintenance ever increasing, intelligent real-time monitoring is imperative to guarantee safe and affordable structures. Two general approaches are currently being investigated in an effort to develop an effective structural health monitoring system for new as well as aging structures. One is the global approach, which measures and analyzes damage-induced changes in the vibrational properties (e.g., modal frequencies and mode shapes). The other is a local approach whereby changes in the characteristics of ultrasonic waves propagating across existing defects or created by emerging defects are measured and analyzed. Both approaches have limitations in their practical implementations, particularly for larger structures [4].

The global approach is only effective in detecting larger defects because the effects of small flaws on the global vibrational properties are generally below the noise level in large structures. Efforts have been made to amplify the differences in the modal properties caused by defects and to eliminate noise using a variety of techniques, including the introduction of system identification and pattern recognition techniques [5–9]. Although the technique is capable of approximately localizing defects (e.g., loss of stiffness) in the vicinity of the measuring devices, its effectiveness in detecting small hidden defects in complex structures remains questionable at present.

The local approach based on ultrasonic wave propagation techniques is highly effective in detecting very small local defects in a variety of structural components. A significant amount of research has been conducted using broadband transducers (notably, PZT) to transmit and receive guided waves (Lamb waves) to detect hidden defects in structural plates. Arrays of built-in piezoelectric patches have been used as sensors and actuators to excite and receive ultrasonic waves in order to characterize the location and extent of structural damage in large structures by analyzing the signal paths [10–15]. However, the current defects-detection methodology suffers from the deterrent effects of ambient noise and, more importantly, it requires extensive involvement of trained operators to analyze the recorded data manually, resulting in extremely time-consuming inspection procedures and strongly operator-dependent conclusions. Since the effectiveness of structural health monitoring systems depends on their ability to detect small defects before they grow to a critical size, it is imperative to invent a method that overcomes these limitations. More specifically, it would be highly beneficial to have a structural health monitoring system characterized by low computational effort, high reliability, and with the ability to analyze the acquired data in near-real time. Such a system could identify a ''perturbed'' area of the structure, provide information about its presence and location, and suggest mitigation strategies to manage the risk.

A recently developed approach is used in this article for fast and efficient damage identification in structural components whereby ultrasonic wave propagation and vibration data are analyzed to determine the location and degree of damage, requiring minimal operator intervention. The collected data are analyzed using a damage index (DI) approach to determine the degree of damage to the structure as a function of time. The DI approach is designed to overcome the complexity and variability of the signals in the presence of damage as well as the geometric complexity of the structure. It relies on the fact that the dynamical properties of a structure change with the initiation of new damage or growth of existing damage. Using measurements performed on an undamaged or partially damaged structure as baseline, the DI is evaluated by comparing the changes in the frequency response of the monitored structure as a new damage occurs or an existing damage grows. Thus, unless the environment undergoes significant changes between the two sets of measurements (which can occur within a very short time frame), noise, in general, will have no effect on the results. Moreover, the proposed algorithm does not require extensive rigorous signal processing, but it computes a single damage parameter (namely, DI) with a high confidence level which makes its very fast and automatic. The DI vanishes if there is no change in the structure and its value increases with the severity and proximity of damage to the sensor locations. Thus if damage is initiated at a location within or near the sensor array, then its location and severity can be determined by the autonomous scheme. The method is applied to identify several types of defects in both metallic and composite panels for different arrangements of the source and the receivers.

2. The DI approach

In this approach, a DI comparing the measured dynamical response of two successive states of the structure is introduced as a determinant of structural damage [16–18]. The dynamic state involved in the definition of the DI at a given sensor location (*control point*) is the frequency response function in the vibration test and the frequency spectrum of the signal in the wave propagation test. The presence of damage modifies the modal properties of the structure as well as certain characteristics of the ultrasonic waves. The changes in the measured dynamic response of the structure are analyzed to reveal the location and degree of damage in the unified approach described below.

Wave propagation and vibration tests are performed in the reference and damaged states of the structure. In the vibration test, forced vibration of the structure is induced by means of suitable actuators in as wide a frequency range as possible. In the wave propagation test, elastic waves with known properties are launched by broadband transducers located on the surface of the structure. The motion produced by the two types of sources is acquired by multiple sensors located on the surface of the structural component.

The damage index, DI, is defined as follows:

$$DI = \left| 1 - \frac{\sum_{f_k=0}^{f_s/2} FD^2(f_k)}{\sum_{f_k=0}^{f_s/2} FI^2(f_k)} \right|, \tag{1}$$

where f_k are the frequencies where the spectra are evaluated, FI and FD the magnitudes of the frequency response functions or spectra for the undamaged and damaged structures, respectively, and f_s the sample rate.

The index can, in principle, be defined for a generic structural parameter including displacement, velocity, acceleration, strain, or voltage measured by embedded or attached sensors. The DI defined in Eq. (1) returns non-zero values only if any change in the measured dynamical response of the structure occurs, and it will return zeros if the experimental measurements are identical.

The reliability of the damage detection procedure is strongly dependent on the reliability of the measured dynamic response of the structure in the reference and damaged states. However, the measurements can be affected by random errors or environmental noise, leading to false or inaccurate results for the DI values. Thus, the tests are repeated several times under the same conditions. In order to correlate the DI values to the presence and degree of damage with a high confidence level, either the collected data are averaged a number of times or a statistical analysis is carried out using the Student's statistic t as described below.

2.1. Statistical DI

Let FI_i be the frequency response function or spectrum of M measurements ($i = 1,\ldots,M$) in the undamaged configuration (baseline). One of these measurements (say $i = 1$) is adopted as reference and the DI defined in Eq. (1) is evaluated for the remaining ($M-1$) measurements at all sensor locations to estimate the threshold values of the damage indices:

$$DI_i^{(1)} = \left| 1 - \frac{\sum_{f_k=0}^{f_s/2} FI_i^2(f_k)}{\sum_{f_k=0}^{f_s/2} FI_1^2(f_k)} \right| \quad i = 2,\ldots,M. \tag{2a}$$

Similarly, let FD_j be the frequency response function or spectrum of N measurements ($j = 1,\ldots,N$) in the damaged configuration. The DI values are calculated using the first frequency response function or spectrum in the undamaged configuration:

$$DI_j^{(2)} = \left| 1 - \frac{\sum_{f_k=0}^{f_s/2} FD_j^2(f_k)}{\sum_{f_k=0}^{f_s/2} FI_1^2(f_k)} \right| \quad j = 1,\ldots,N. \tag{2b}$$

A coupled Student's Test [19–20] is applied to verify that these M and N measurement sets belonged to different structural configurations, with a confidence level higher than 95%. The statistic t is defined

as follows:

$$t = \frac{|\overline{DI^{(1)}} - \overline{DI^{(2)}}|}{\sqrt{A \cdot B}}, \tag{3}$$

where

$$A = \frac{(M-1)+N}{(M-1)\cdot N}; \quad B = \frac{[(M-2)\sigma_1^2 + (N-1)\sigma_2^2]}{[(M-1)+N-2]}. \tag{4}$$

In Eq. (3), $\overline{DI^{(1)}}$ and $\overline{DI^{(2)}}$ are the means of the two sets of $\overline{DI_i^{(1)}}$ and $\overline{DI_j^{(2)}}$ related to the healthy and damaged configurations, respectively; σ_1 and σ_2 are their standard deviations, and $M-1$ and N represent the number of samples for the two sets. The number of "degrees of freedom", v of the T-test is a function of $M-1$ and N ($v = M-1+N-2$) and is related to the "confidence level" of each test. If $M = 5$ and $N = 5$, then $v = 7$, and for a confidence level of 0.975, $t_{0.975} = 2.36$. This means that if the statistic t value calculated from Eq. (3) is greater than 2.36, then the difference between the means of the compared data sets is not caused by random error, but is due to real changes in the physical properties of the structure.

3. Wave propagation-based damage detection and localization

3.1. Experimental setup

The general experimental setup used for the test cases is shown in Fig. 1. Several identical broadband PZT transducers (B1025, Digital Wave) with 5 MHz center frequency placed on the plate surface were used as transmitters and receivers of the waves. The transmission of ultrasound was aided by the application of an ultrasonic gel couplant (Sonotech). The source signal was a 10 V peak-to-peak single sine pulse generated by an arbitrary waveform generator (33220A, Agilent). A four channel signal conditioner (Digital Wave Corp., Model FM-1) was used to boost the signal strength in all the experiments. The ultrasonic signal was digitized and recorded directly in a four-channel digital oscilloscope with 100 MHz sampling rate (54624A, Agilent). The digital ultrasonic signals were then downloaded directly to a personal computer for post processing via a GPIB interface.

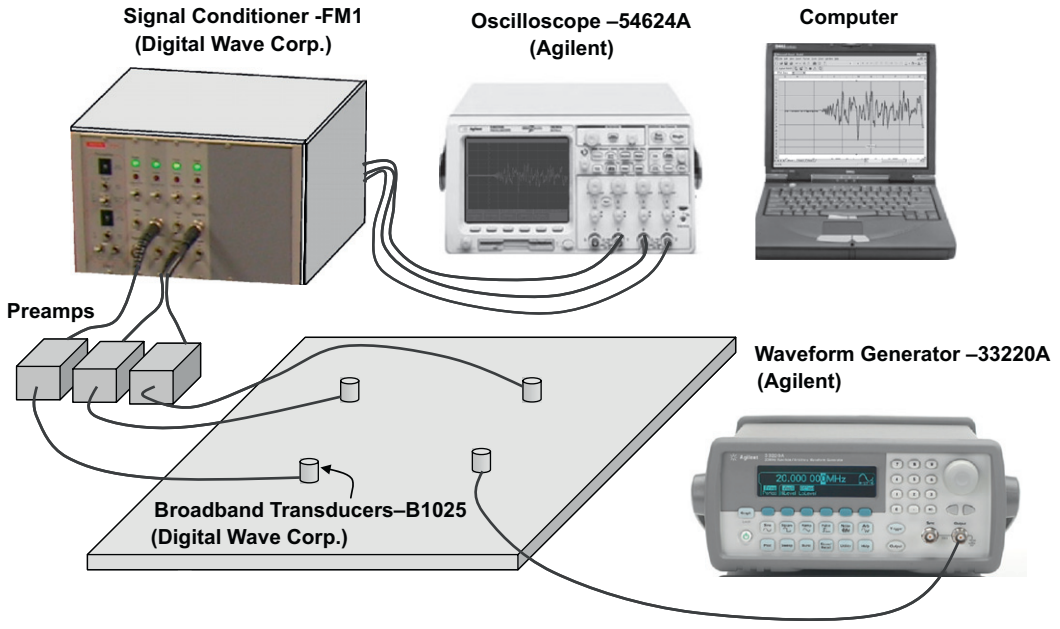

Fig. 1. The experimental setup used for wave propagation-based damage identification.

3.2. Results

3.2.1. Investigations on an aluminum plate

In order to comprehend the effectiveness of the statistical DI approach using wave propagation technique, a simple case of an aluminum plate with a through hole is presented first as representative of loose rivet holes. The overall test configuration of this study is shown in Fig. 2. The aluminum plate of dimensions 419.1 mm × 368.3 mm × 1.59 mm (16.5 in × 14.5 in × 1/16 in) was investigated with twelve control points, which can be used as an actuator as well as a sensor location. The sensor and actuator configuration of the investigated seventy actuator-sensor paths is summarized in Table 1. The numbering scheme for the actuator and the sensor listed in the table is consistent with that of the piezo-electric elements in Fig. 2. The excitation signal (source) was a 750 kHz-1cycle sinusoidal pulse. First, the baseline signals corresponding to seventy two different actuator and sensor paths were recorded at a known intact condition of the plate. For a given

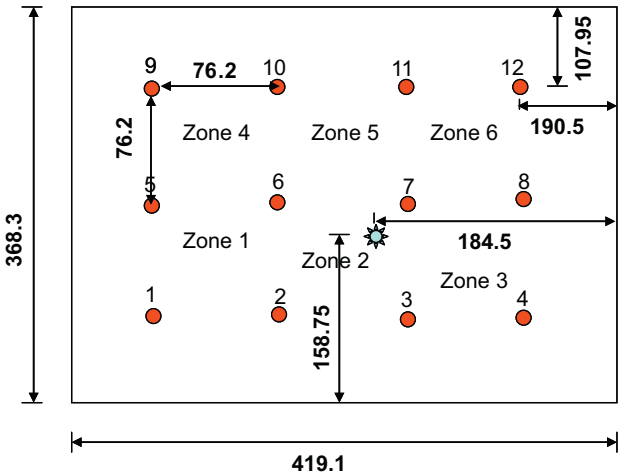

Fig. 2. Layout of the actuators/sensors on the aluminum plate. The location of the through hole is also shown. All dimensions are in mm. '●' Actuator/Sensor location and '✹' damage location.

Table 1
Sensor and actuator configuration of the 72 measurement paths.

Actuator	Sensor	Path	Actuator	Sensor	Path	Actuator	Sensor	Path	Actuator	Sensor	Path
1	3	1	4	5	19	7	1	37	10	2	55
1	6	2	4	6	20	7	2	38	10	3	56
1	7	3	4	7	21	7	3	39	10	4	57
1	8	4	4	9	22	7	6	40	10	6	58
1	11	5	4	10	23	7	10	41	10	7	59
1	12	6	4	11	24	7	11	42	10	11	60
2	3	7	5	3	25	8	1	43	11	1	61
2	6	8	5	4	26	8	2	44	11	2	62
2	7	9	5	6	27	8	3	45	11	3	63
2	8	10	5	7	28	8	5	46	11	4	64
2	11	11	5	8	29	8	6	47	11	6	65
2	12	12	5	11	30	8	7	48	11	7	66
3	6	13	6	3	31	9	2	49	12	1	67
3	7	14	6	4	32	9	3	50	12	2	68
3	8	15	6	7	33	9	4	51	12	3	69
3	10	16	6	8	34	9	6	52	12	6	70
3	11	17	6	11	35	9	7	53	12	7	71
3	12	18	6	12	36	9	11	54	12	10	72

measurement path, baseline signal was recorded four times (i.e., $M = 4$ as discussed in Section 2.1). A through hole of 3.175 mm (1/8 in) was drilled at the location shown in Fig. 2 and the wave propagation tests were then repeated four times in presence of the defect as that in the intact configuration. The sensors and actuators were removed and replaced during concurrent measurements. Typical recorded signals and their spectra in presence and absence of the drilled hole are presented in Fig. 3 for measurement path nine. The differences in the signals and their spectra are caused by reflection, scattering, and diffraction of the waves by the damaged region. Careful model-based analysis of the signals can, in principle, be used to determine the nature, location, and severity of the damage [21], however, would involve extensive manual intervention. Thus, the statistical DI approach offers a more pragmatic approach for approximately locating and characterizing the damage.

The statistic t, defined in Eq. (3) are computed instantly for each path from the measured data and plotted in Fig. 4. In this case, a confidence level of 97.5% is used for which the statistic t is equal to 2.57. A given measurement path is classified as damaged when the value of the statistic t becomes larger than 2.57, which is noted to be the threshold value for this test. In Fig. 5(a), the measurement paths that have statistic t values greater than 2.57 are displayed by solid arrow lines. The direction of the wave motion from actuator to sensor is indicated by the tip of the arrow. From the plot of the measurement paths (Fig. 5a), it is envisioned that the damage appears in the region (zone 2), which has maximum number of measurement paths crossing each

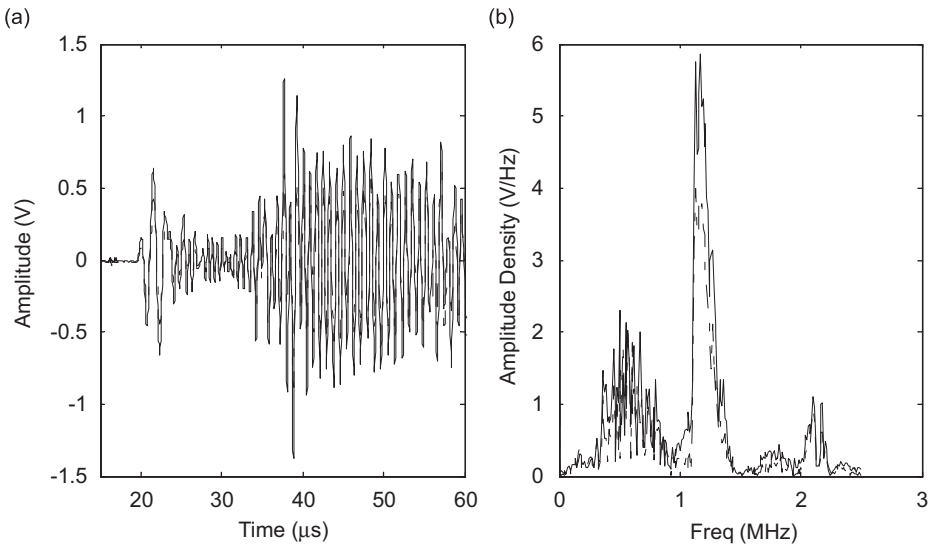

Fig. 3. Typical recorded signals (a) and their spectra (b) for measurement path 9, i.e., the source and the receiver are located at 2 and 7, respectively. A part of the recorded signal is shown in the figure. '—' undamaged signal and '- - -' damaged signal.

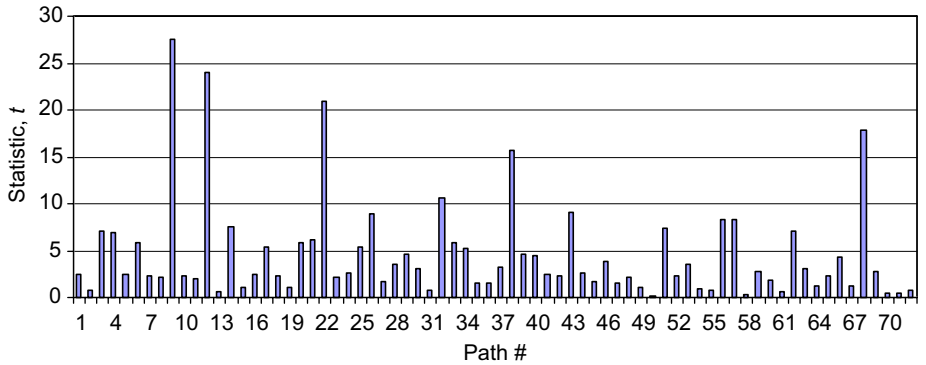

Fig. 4. Values of the damage parameter (statistic, t) for different measurement paths in Table 1.

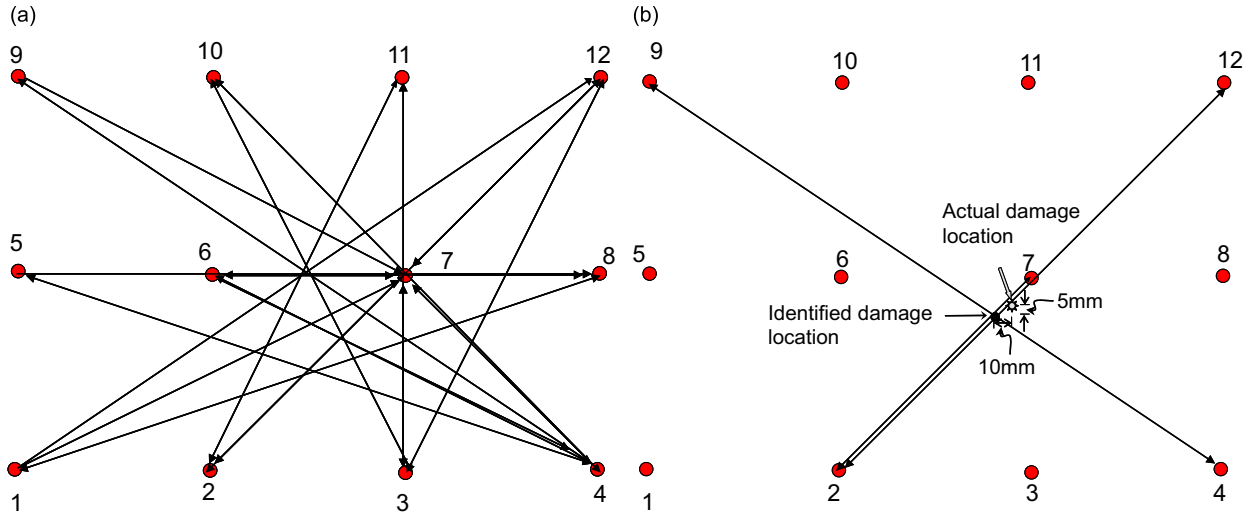

Fig. 5. (a) Representation of measurement paths with statistic t values greater than the threshold value of 2.57 and (b) measurement paths with top five statistic t value showing the identified damage location.

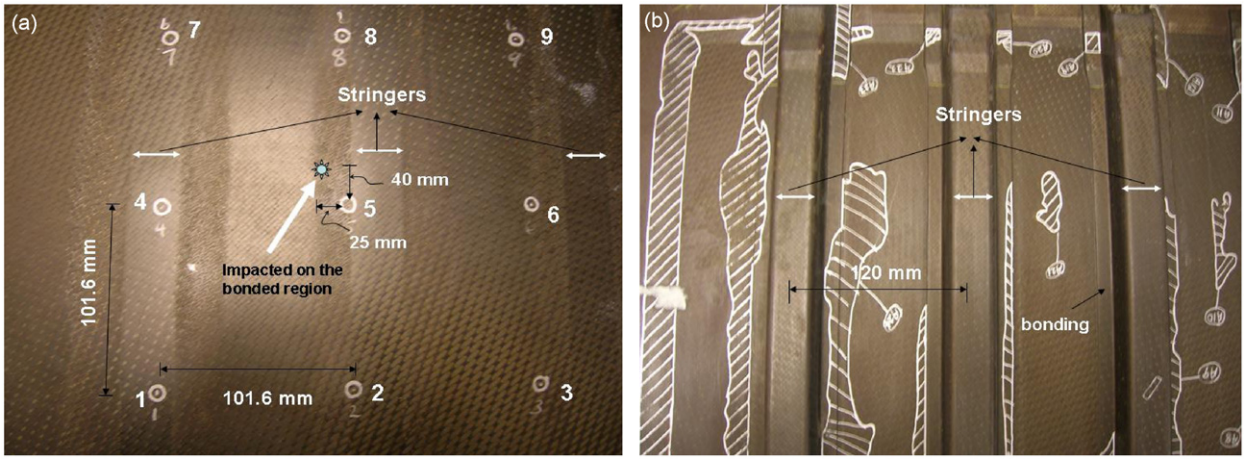

Fig. 6. (a) Top view of the stiffened composite panel showing the stringers, transducers and impact locations and (b) back view of the stiffened panel showing the stringers and the bonded regions.

other. In order to identify the damage location more accurately, the measurement paths with top five statistic t values are retained in Fig. 5(b). In general, it is observed that the value of the statistic t is significant, if the defect falls right on the measurement paths. The approximate location of the defect is shown in Fig. 5(b). A similar damage location identification method was applied earlier [11] using a virtual mesh (grid) to locate the damage. It is concluded that a large number of sensors are required to locate the damage precisely. It should also be noted that the peak value of the statistic can be correlated to the size of the defect through a more detailed numerical modeling and experiments with a large number of specimens containing different sized defects.

3.2.2. Investigations on a stiffened composite panel

The effectiveness of the approach is now examined for a graphite/epoxy stiffened composite panel (800 mm × 600 mm × 2 mm) made out of resin infusion technique and has five stringers bonded onto the plate. The geometric and material complexities of the structure present practical difficulties in the direct analysis of both wave propagation and modal vibration data using theoretical constructs. The test was conducted at one

corner of the plate using nine transducers glued on the top of the plate at a spacing of 101.6 mm (4 in), as shown in Fig. 6a. The back view of the test spot shows a clear picture of the three stringers and how they are bonded to the plate (Fig. 6b).

Ultrasonic tests were performed four times in the intact configuration, where fifty four measurement paths was used as shown in Table 2 and 500 kHz-1 cycle sinusoidal pulse was used as an excitation signal (source). A customized impact tester with a breaking mechanism was used to perform the impact tests. An impactor assembly of total weight 10.6 kg (23.35 lb) was dropped from a height of 0.61 m (2 ft) at one of the bonded regions as shown in Fig. 5a. After the impact test, the exterior surface of the impact plate was inspected. There was no visible marking or scratch on the surface of the composite plate after the impact test. C-scans were performed around the vicinity of the impact location before and after the impact test (Fig. 7). The C-scan results clearly show the appearance of delamination after the impact test. Ultrasonic tests were then repeated four times as that of the intact configuration, and the received signals and their spectra is shown in Fig. 8 for

Table 2
Sensor and actuator configuration of the 54 measurement paths.

Actuator	Sensor	Path	Actuator	Sensor	Path	Actuator	Sensor	Path
1	2	1	4	1	19	7	1	37
1	4	2	4	2	20	7	2	38
1	5	3	4	5	21	7	5	39
1	6	4	4	3	22	7	3	40
1	8	5	4	6	23	7	4	41
1	9	6	4	9	24	7	6	42
2	1	7	5	1	25	8	1	43
2	4	8	5	2	26	8	2	44
2	5	9	5	4	27	8	4	45
2	7	10	5	3	28	8	3	46
2	8	11	5	6	29	8	5	47
2	9	12	5	7	30	8	7	48
3	1	13	6	1	31	9	1	49
3	2	14	6	2	32	9	2	50
3	4	15	6	4	33	9	3	51
3	5	16	6	5	34	9	4	52
3	7	17	6	7	35	9	5	53
3	8	18	6	8	36	9	6	54

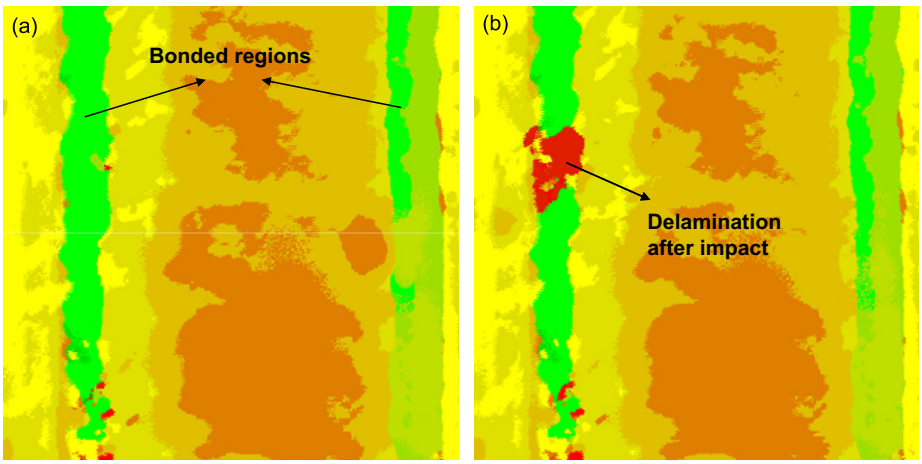

Fig. 7. C-scan of the impacted region: (a) before impact test and (b) after impact test.

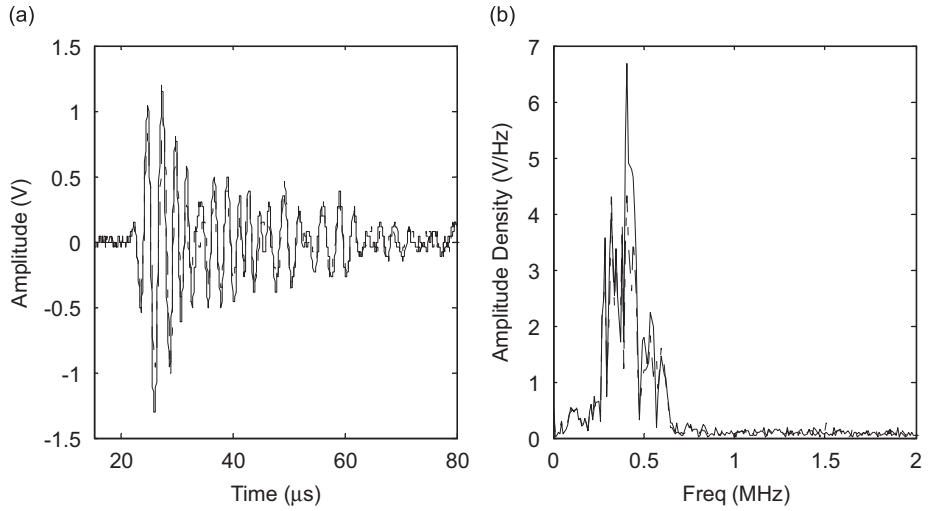

Fig. 8. Typical recorded signals (a) and their spectra (b) for measurement path 30, i.e., the source and the receiver are located at 5 and 7, respectively. A part of the recorded signal is shown in the figure. '—' pre-impact signal and '---' post-impact signal.

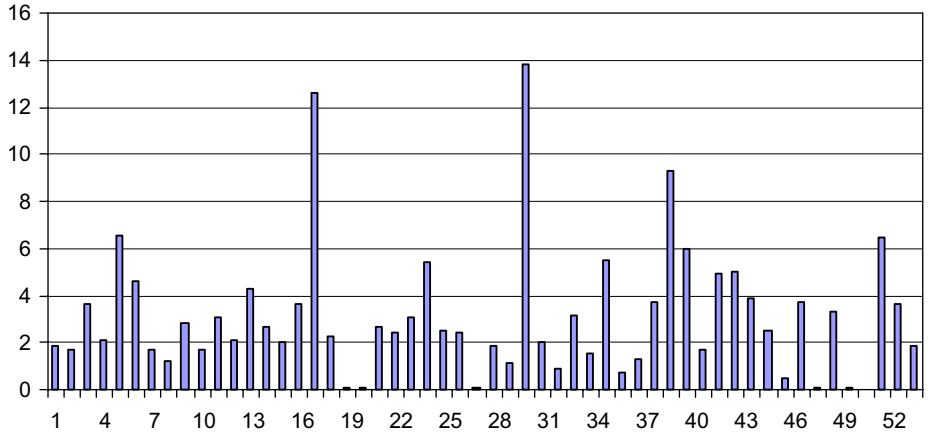

Fig. 9. Values of the damage parameter (statistic, t) for different measurement paths in Table 2.

the measurement path thirty. The damage caused by impact is extremely complex and the solution of even the direct problem of wave interaction with the damaged region is not found in literature.

The computed statistic t for each measurement path is plotted in Fig. 9. In Fig. 10(a), the measurement paths that have statistic t values greater than 2.57 are displayed by solid arrow lines. The displayed measurement paths confirm the appearance of damage in zone 4. Measurement paths with top five statistic t values are then retained in Fig. 10(b), which identifies the damage location with some confidence. It will always be necessary to carry out a more detailed test of the identified area using local NDE methods. Even the approximate localization that can be achieved by a small sensor array has the potential to dramatically improve state of the art of damage detection in large structures.

4. Vibration-based damage detection and localization

The technique implemented here is based on the comparison between the frequency response functions [22,23] of the healthy structure at time t (a baseline), and the frequency response functions collected at time $t+\Delta t$, after a damage occurred. When a structure is excited at a generic location with an arbitrary input signal

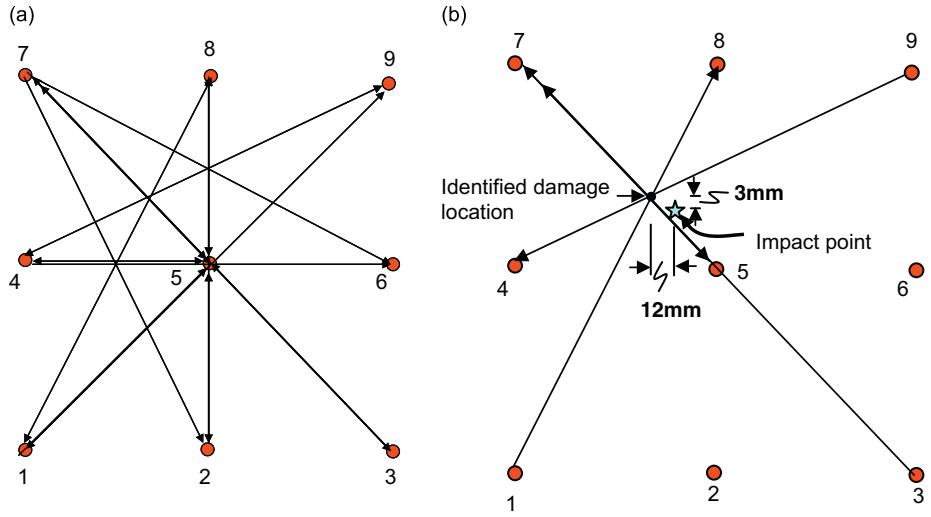

Fig. 10. (a) Representation of measurement paths with statistic t values greater than the threshold value of 2.57 and (b) measurement paths with top five statistic t value showing the identified damage location.

and the measurement of the output response is made at another point, the two signals are time dependent. The complex Fourier transforms of the input and output signals are denoted by $X(f)$ and $Y(f)$, respectively where f is the frequency and the frequency response function of the structure is calculated with the following estimator in order to reduce the noise on the output uncorrelated with the input:

$$\mathrm{FRF}(f_k) = \frac{\hat{G}_{xy}}{\hat{G}_{xx}}, \tag{5}$$

where $\hat{G}_{xy}(f_k)$ is an estimate of the cross-spectrum between the functions $Y(f)$ and $X(f)$:

$$\hat{G}_{xy}(f_k) = \frac{1}{KK}\sum_{kk=1}^{KK}\left[\frac{{}^{kk}X_k^{*kk}Y_k}{f_s^2}\right], \tag{6}$$

where ${}^{kk}X_k^*$ is the complex conjugate of the discrete Fourier transform of the kkth sampled time history input signal, ${}^{kk}Y_k$ is the discrete Fourier transform of the kkth sampled time history output signal, f_s is the sample rate and f_k the frequencies at which the spectrum is evaluated and $\hat{G}_{xx}(f_k)$ is an estimate of the auto-spectrum of $X(f)$ defined by

$$\hat{G}_{xx}(f_k) = \frac{1}{KK}\sum_{kk=1}^{KK}\left[\frac{{}^{kk}X_k^{*kk}X_k}{f_s^2}\right]. \tag{7}$$

When the damage appears, the stiffness, damping and sometimes the density (e.g., when corrosion is involved) of the structural component change, causing changes in the frequency response functions, as shown in Fig. 11. Since the dynamic response of a system is related to the stiffness, damping and mass distributions, vibration measurements can be used to detect such changes.

Based on the assumption that it is always possible to determine the frequency response functions of a structure using a linear combination of its modal response, one can in principle relate the changes in the frequency response function to those in the modal parameters (modal frequencies, mode shapes and their residuals) within the same frequency domain. For both the modal and frequency response function approaches (based on frequency response function comparison), it is necessary to refer the health status of the monitored structure to an index. For the modal approach the index chosen here refers to the spatial correlation of the corresponding mode shapes before and after the structural perturbation occurs, whereas for the frequency response function approach the index refers to a frequency cross-correlation of the response functions before and after the perturbation occurs. The two approaches can be compared and should provide

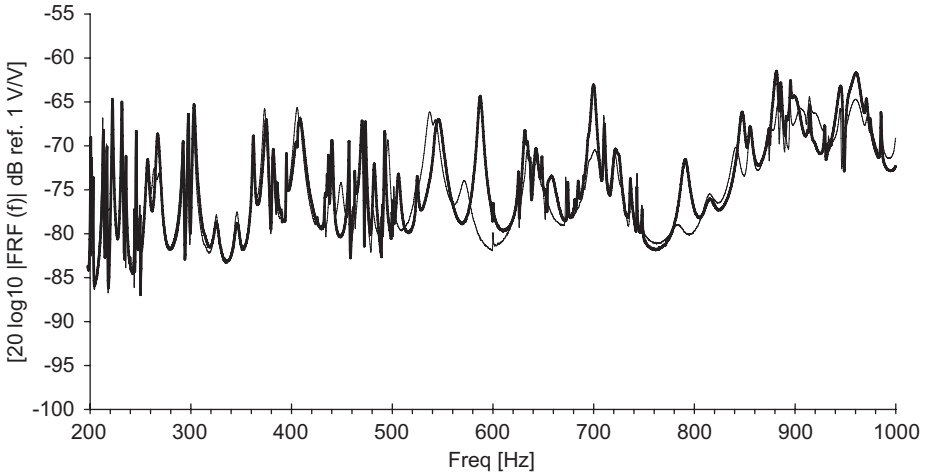

Fig. 11. The magnitude of the frequency response functions for the healthy (thick line) and the damaged (thin line) panel.

the same information (healthy or damaged status) if applied in the same frequency domain. An experimental work carried out on a woven composite plate and aimed at such comparison is presented later on.

Since the procedure is dependent upon the reliability and accuracy of the frequency response function acquisition process, each frequency response function is averaged at least three times in order to reduce noise due to unknown effects in characteristic times lower then the data acquisition rate. Moreover, the frequency correlation between the input and output signals is monitored through the use of the Coherence Function (CF) [22,23] between them defined by

$$\mathrm{CF}^2(f) = \frac{|\hat{G}_{xy}(f)|^2}{\hat{G}_{xx}(f)\hat{G}_{yy}(f)}. \tag{8}$$

It can be seen that $0 \leqslant \mathrm{CF}^2(f) \leqslant 1$, with the lower value zero corresponds the no frequency correlation between the input and output signals while the value one indicates perfect frequency correlation between the two signals.

4.1. Experimental setup

Piezoelectric patches were employed both as sensors and actuators in order to implement the described health monitoring approach. Each patch was used sequentially as an actuator while all the others collect the response signals. In order to provide adequate excitation, a voltage amplifier was introduced between the output channel of the acquisition system and the patch acting as actuator. The chosen amplifier was produced by the TREK company and was able to amplify the input signal by a factor of 25 in the frequency range 0–20 kHz. The details of the experimental setup can be found in [18].

The influence of the sensor characteristics was evaluated by comparing the results obtained from the piezoelectric patches as sensors, described in the above paragraph, with those obtained by employing a laser vibrometer. A Polytec PSV-400 laser vibrometer was used as a sensor in order to acquire the response at a number of points over the test article. The device measures the two-dimensional distribution of the velocity on the surface of the structure based on laser interferometry. The main advantage of the laser vibrometer sensor is the improved sensitivity and the possibility to perform a dense, fast, automatic and non-intrusive scanning over the test article, as no other piezo-patch is required except the one working as the actuator.

4.2. Results

To demonstrate the improvement in the damage detection technique, a comparative test was carried out on a simple unstiffened woven composite plate (530 mm × 530 mm × 3 mm) shown in Fig. 12. A reversible

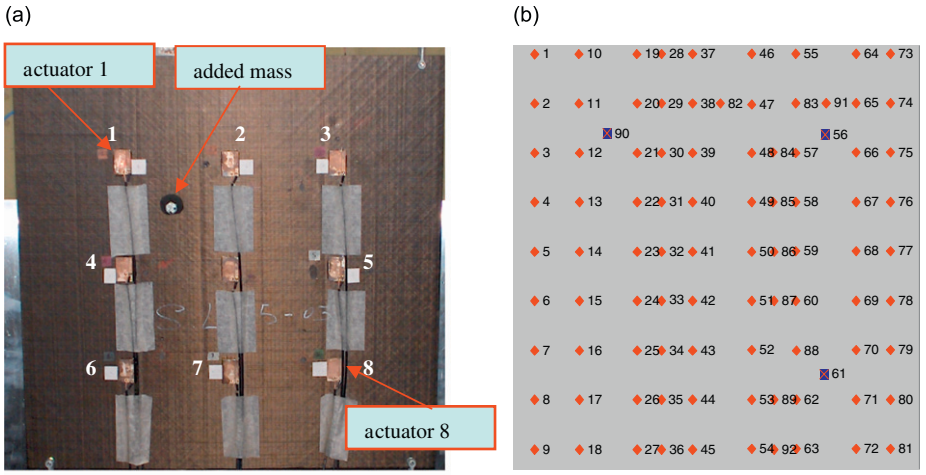

Fig. 12. The laser vibrometer Polytec PSV-400 scanning setup for composite panel: (a) the damage has been simulated with a 20 g mass added. The piezo-patches are also numbered and (b) schematic of the laser beam acquisition points.

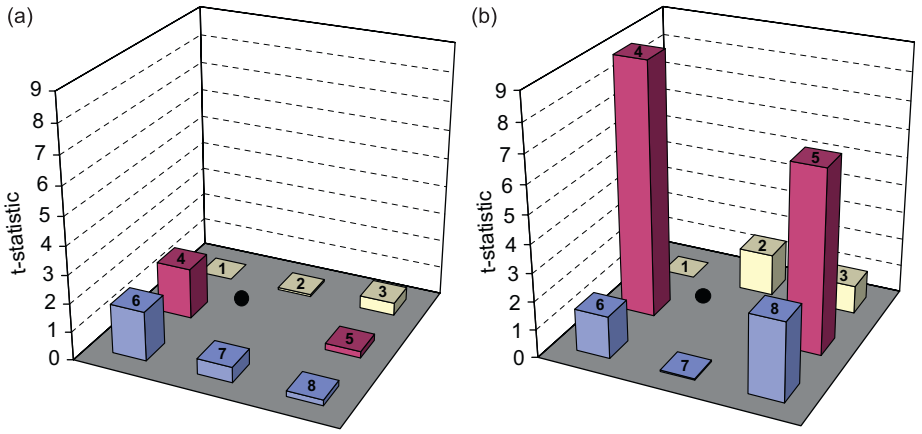

Fig. 13. The statistic t evaluated over the unstiffened panel using piezo patches (a) and the laser vibrometer (b) as sensors. The comparison has been carried out by measuring the responses at 8 points. The damage is located at the black solid circle.

damage was simulated with a 20 g mass added to the panel. Actuator 1 was used to excite the structure, and the healthy and damaged frequency response functions were measured with both the piezo-patches and laser vibrometer at other seven locations (see Fig. 12), for the same baseline and damaged configuration. In both cases the signal provided by the amplifier to the piezo-patch acting as a source was employed as input function. The voltage measured by the piezo-patch acting as a sensor was considered as output function, whereas the velocity measured by the vibrometer was considered as output function. The laser vibrometer acquisitions were made at eight locations as close as possible to the piezo-patches for comparison purposes. Using the DI and statistic formulation described in Section 2, the results are reported in the Figs. 13 and 14.

The comparison of the statistics t evaluated using both the piezo-patches and the laser vibrometer as sensors in Fig. 13 shows that the latter "sensor" is more efficient in damage prediction, as it gives higher values of t meaning higher confidence levels in damage localization. The laser vibrometer is next used to construct the DI map by performing only one scan for ninety two acquisition points over the panel for both the healthy and damaged configurations. Fig. 14 shows the accuracy of the predicted "damage" location through the distribution of the DI over the panel.

The responses measured by the laser vibrometer was employed to extract the modal parameters (natural frequencies and modal shapes) in the frequency range 150–1000 Hz and to calculate the DI from Eq. (1) over

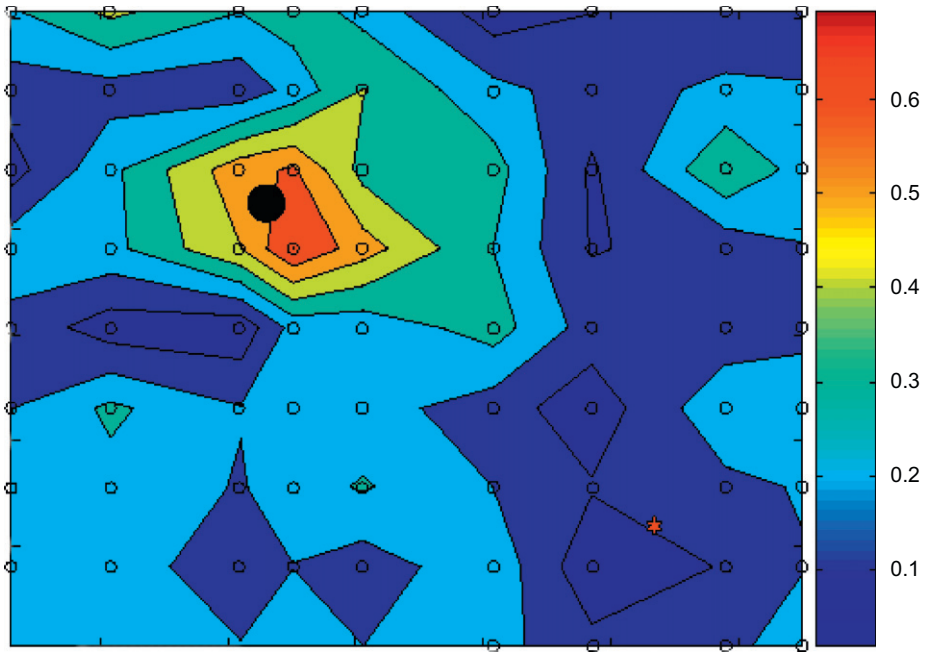

Fig. 14. Damage index distribution over the panel (frequency range 150–1000 Hz). The 92 small circles represent the acquisition points. The 20 g added mass is located at the black solid circle.

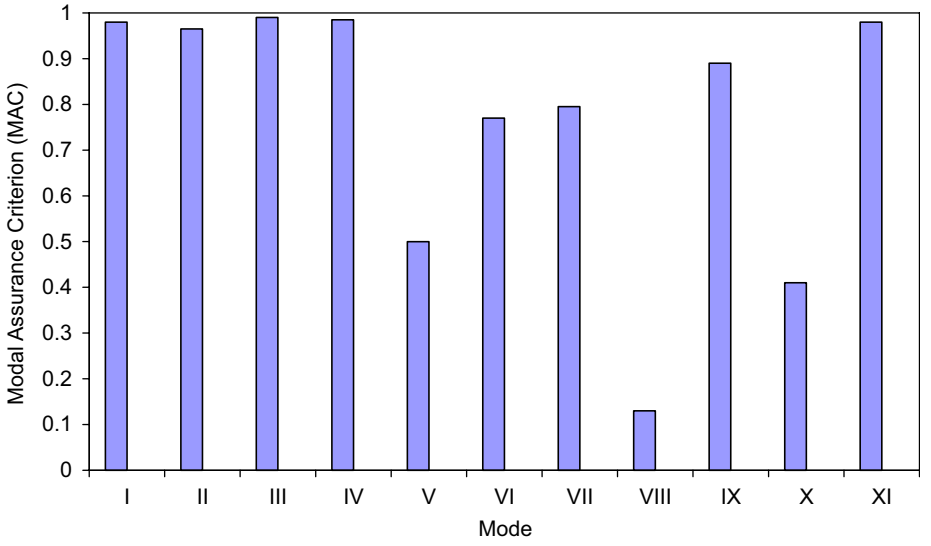

Fig. 15. The Modal Assurance Criterion (MAC) evaluated with the excitation provided by the actuator 1 (see Fig. 12) for the panel with (damaged) and without (healthy) the added mass. The frequency range is 150–1000 Hz.

different frequency ranges. Furthermore, in order to spatially correlate the modal shapes at each corresponding natural mode on the healthy and damaged structure, the Modal Assurance Criterion (MAC) [22] was employed. The MAC is generally used to evaluate the modal correlation (i.e., the correlation between the modal parameters) between numerical analyses and experimental tests, but it is possible to use it to quantify the variation in the modal parameters regardless of the type of test employed (numerical or experimental). In the present work the MAC was used to compare and quantify the changes in the modal parameters evaluated from the measurements carried out on the healthy and damaged structure.

The following expression was used:

$$\mathrm{MAC}(\boldsymbol{\psi}_\mathbf{n}, \boldsymbol{\psi}_\mathbf{e}) = \frac{|\boldsymbol{\psi}_\mathbf{n}^t \cdot \boldsymbol{\psi}_\mathbf{e}|^2}{(\boldsymbol{\psi}_\mathbf{n}^t \cdot \boldsymbol{\psi}_\mathbf{e})(\boldsymbol{\psi}_e^t \cdot \boldsymbol{\psi}_n)}, \tag{9}$$

where $\{\psi_n\}$ and $\{\psi_e\}$ are the healthy and damaged eigenvectors (mode shapes) at corresponding modes, respectively. The MAC returns a value ranging from zero (no correlation) to one (full correlation) and a value of 0.9 ensures a reasonably good experimental correlation, indicating that no change in the modal parameters implies the absence of damage to the structure. Figs. 15 and 16 and Table 3 show that the MAC values predict a good correlation up to about 500 Hz for two different excitation locations, actuators 1 and 8, respectively. As an example, the plots of the fifth mode for both the healthy and the damaged panel are presented in Fig. 17.

Figs. 18 and 19 show the values of the DI calculated in the two frequency band-widths 150–500 Hz and 500–1000 Hz, respectively. It should be noted that, in good agreement with the modal approach, the frequency response functions approach can detect damage at frequencies higher than 500 Hz, further demonstrating the advantage of locating the structural perturbation by the simple analysis of the DI map.

From the comparison of Figs. 14, 18 and 19, it can be seen that when the analysis is carried out in the frequency range 150–500 Hz the damage detection and localization is not achievable from the DI formulation (Fig. 18). This is in agreement with the good correlation given by the MAC (see Figs. 15 and 16). In other words the damage (added mass) does not produce an appreciable effect below 500 Hz. From 500 Hz up to

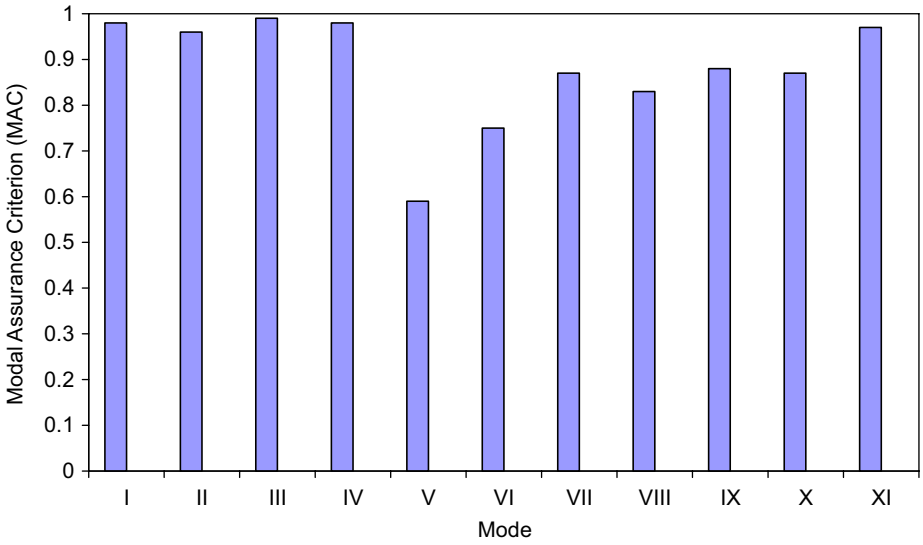

Fig. 16. The Modal Assurance Criterion (MAC) evaluated with the excitation provided by the actuator 8 (see Fig. 12) for the panel with (damaged) and without (healthy) the added mass. The frequency range is 150–1000 Hz.

Table 3
Natural frequencies in the range 150–1000 Hz for both the healthy and damaged woven composite panel.

Act 1	I	II	III	IV	V	VI	VII	VIII	IX	X	XI
Healthy (Hz)	177.8	192.2	303.4	375.0	545.3	586.8	699.3	791.8	815.3	846.5	855.9
Damaged (Hz)	177.5	187.8	302.5	373.4	543.1	571.8	695.6	787.1	815.3	844.8	855.6
Act 8	I	II	III	IV	V	VI	VII	VIII	IX	X	XI
Healthy (Hz)	178.1	192.1	303.1	374.3	546.5	586.8	700.0	790.8	815.3	847.5	855.6
Damaged (Hz)	177.5	187.5	302.5	373.1	543.1	571.8	698.1	783.7	815.3	841.2	855.3

The excitation is provided by the actuators 1 and 8.

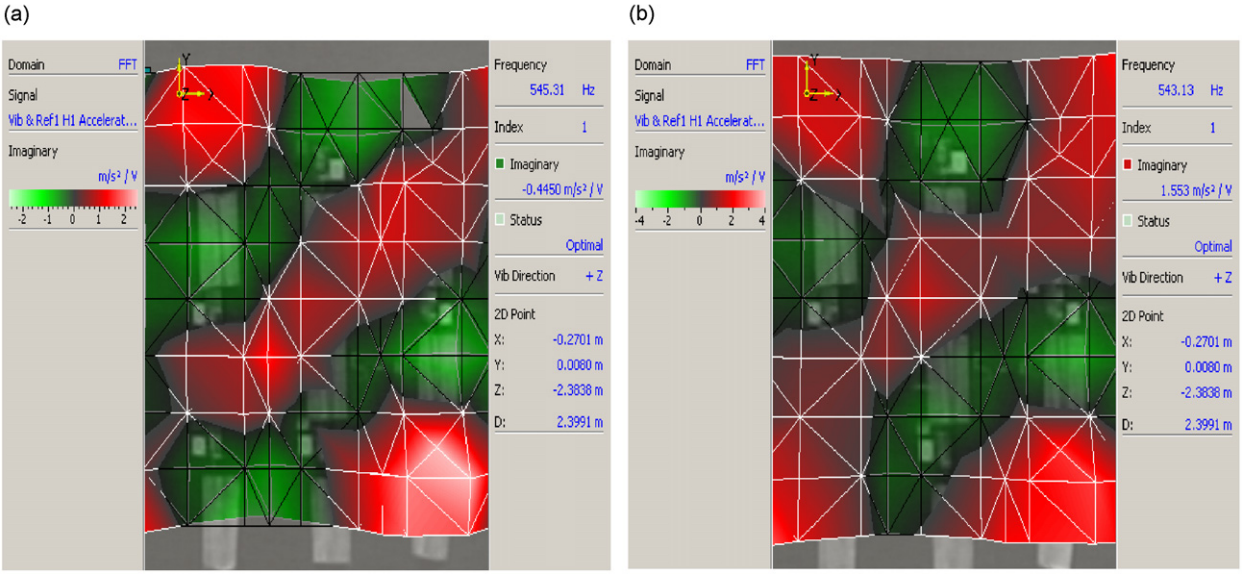

Fig. 17. Representation of the 5th mode for the healthy (a) and damaged (b) panel. Data collected using the laser vibrometer have been used.

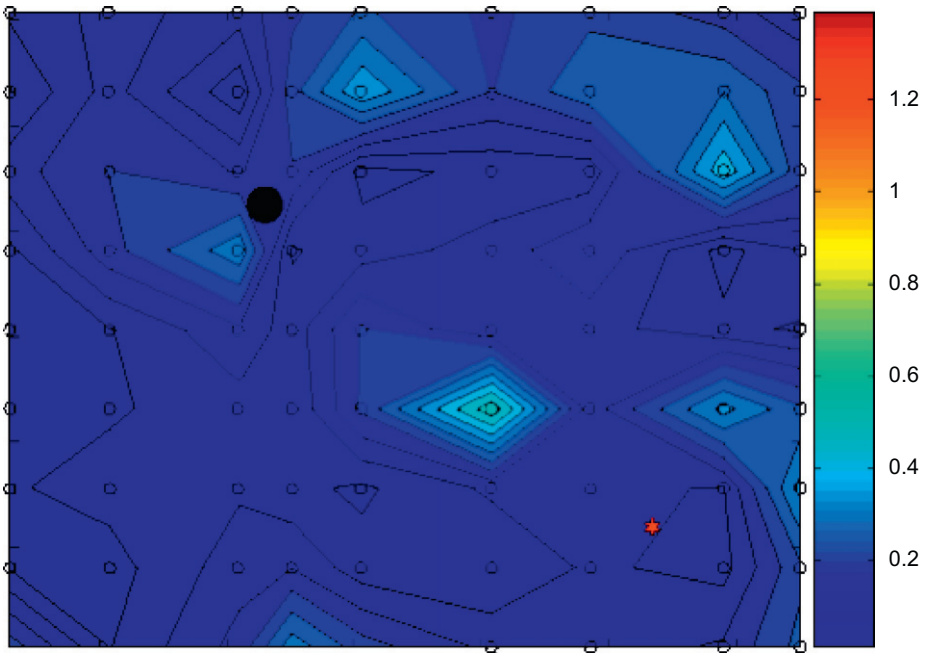

Fig. 18. Damage index distribution over the panel (frequency range 150–500 Hz). The small circles represent the acquisition points. The 20 g added mass is located at the black solid circle. The excitation is provided by the actuator 8.

1 kHz a poor modal correlation is found (see Figs. 15 and 16) and consequently the DI distribution over the panel provides a clear localization of the damage (see Fig. 19). Finally, it is worth noting by comparing Figs. 14 and 19 that even performing the DI evaluation over the entire frequency domain, where some modes are well correlated to each other and some others do not, a good estimation of the damage location can be achieved.

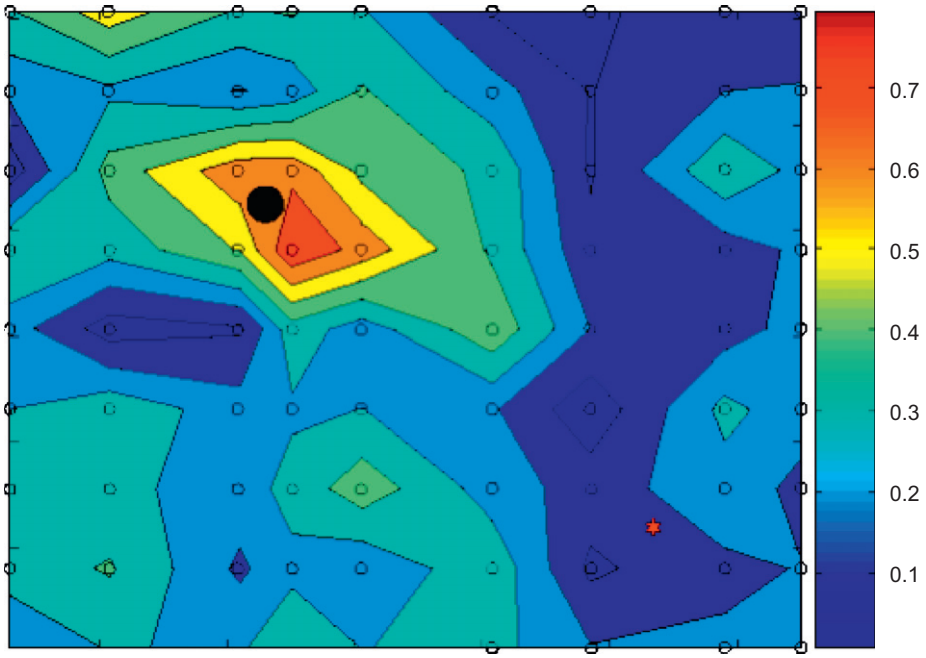

Fig. 19. Damage index distribution over the panel (frequency range 500–1000 Hz). The small circles represent the acquisition points. The 20 g added mass is located at the black solid circle. The excitation is provided by the actuator 8.

5. Concluding remarks

The damage index approach presented here can be used for structural condition monitoring of a variety of aerospace and civil structures, including aircraft, spacecraft, ships, bridges, automobiles, etc. The present study clearly illustrates the potential effectiveness of the statistical damage index approach to predict the approximate location and severity of the damage from a large dataset collected by a network of distributed sensors and actuators in relatively complex structures with minimal manual intervention. While no attempt was made here to automate the graphical representation of the identified damage location/severity, it would be a simple matter to automate the identification of the peaks in the indices and the locations in the instrument array. The proposed approach thus makes it possible to identify very small areas of damage with a high level of reliability. While the vibration-based analysis is expected to identify widespread damage within the structure, analysis of the waveform signals would provide more detailed information on the location and nature of smaller defects. The approach presented here can be very useful in the development of an automated continuous structural health or condition monitoring system because of its simplicity and minimal requirement for operator involvement. This ability should result in major reductions in the cost of sustaining current and future advanced structures, extend the service life of aging aircraft fleet, and provide new capabilities for improving structural safety and reliability. Practical implementation of the technique in real structures will, however, require additional research involving laboratory tests and theoretical modeling, decisions on areas to be instrumented, installation of denser sensor arrays and refinement of algorithm for real time applications.

Acknowledgments

S. Banerjee wishes to acknowledge the partial support from the Missouri Transportation Institute (Grant no. DTOS59-06-00035) and the ultrasonic facilities provided at the non-destructive testing lab at the Parks College of Engineering, Aviation and Technology, Saint Louis University. Vibration-based activities described in the paper have been developed within the research project named M.E.S.E.M.A. (Magnetoelastic Energy

Systems for Even More Electric Aircraft) funded by the European Commission and coordinated by the Department of Aerospace Engineering of the University of Naples "Federico II".

References

[1] J.N. Kudva, M.J. Grage, M.M. Roberts, Aircraft structural health monitoring and other smart structures technologies—perspectives on development of smart aircraft, *Proceedings of the 2nd International Workshop on Structural Health Monitoring*, Stanford, September 1999, pp. 122–132.
[2] *Aging of US Air Force Aircraft*, Publication NMAB-488-2, National Academy Press, Washington, DC, 1997.
[3] P.C. Chang, A. Flatau, S.C. Liu, Review paper: health monitoring of civil infrastructure, *Structural Health Monitoring* 2 (2003) 257–267.
[4] A.K. Mal., Structural health monitoring, *Mechanics: American Academy of Mechanics* 33 (11–12) (2004).
[5] Y. Zou, L. Tong, G.P. Steven, Vibration based model-dependent damage (delamination) identification and health monitoring for composite structures—a review, *Journal of Sound and Vibration* 2 (2000) 357–378.
[6] G. Park, H. Cudney, D.J. Inman, Impedance-based health monitoring of civil structural components, *ASCE Journal of Infrastructure Systems* 6 (2000) 153–160.
[7] K. Worden, G. Manson, D. Allman, Experimental validation of a structural health monitoring methodology: part I. Novelty detection on a laboratory structure, *Journal of Sound and Vibration* 259 (2003) 323–343.
[8] S.S. Kessler, S.M. Spearing, M.J. Atalla, C.E.S. Cesnik, C. Soutis, Damage detection in composite materials using frequency response methods, *Composites Part B* 33 (2002) 87–95.
[9] S.K. Thyagarajan, M.J. Schulz, P.F. Pai, J. Chung, Detecting structural damage using frequency response functions, *Journal of Sound and Vibration* 210 (1998) 162–170.
[10] Z. Su, L. Ye, Y. Lu, Guided Lamb waves for identification of damage in composite structures: a review, *Journal of Sound and Vibration* 295 (2006) 753–780.
[11] J. Park, F.K. Chang, Built-in detection of impact damage in multi-layered thick composite structures, *Proceedings of the 4th International Workshop on Structural Health Monitoring*, Stanford, September 2003, pp. 1391–1398.
[12] H. Sohn, G. Park, J.R. Wait, N.P. Limback, C.R. Farrar, Wavelet-based active sensing for delamination detection in composite structures, *Smart Materials and Structures* 13 (2004) 153–160.
[13] V. Giurgiutiu, A. Cuc, Embedded NDE for structural health monitoring, damage detection, and failure prevention, *Shock and Vibration Digest* 37 (2005) 83–105.
[14] X. Qing, S. Beard, A. Kumar, H. Chan, R. Ikegami, Advances in the development of built-in diagnostic system for filament wound composite structures, *Composite Science and Technology* 66 (2006) 1694–1702.
[15] W.J. Staszewski, C. Boller, S. Grondel, C. Biemans, E. O'Brien, C. Delebarre, G.R. Tomlinson, Damage detection using stress and ultrasonic waves, in: W.J. Staszewski, C. Boller, G.R. Tomlinson (Eds.), *Health Monitoring of Aerospace Structures*, Wiley, Chichester, 2004, pp. 125–162.
[16] S. Banerjee, F. Ricci, F. Shih, A.K. Mal, Structural health monitoring using ultrasonic guided waves, in: T. Kundu (Ed.), *Advanced Ultrasonic Methods for Material and Structure Inspection*, ISTE, London and Newport Beach, California, 2007, pp. 43–86.
[17] A.K. Mal, F. Ricci, S. Banerjee, F. Shih, A conceptual structural health monitoring system based on vibration and wave propagation, *Structural Health Monitoring* 4 (2005) 283–293.
[18] S. Banerjee, F. Ricci, E. Monaco, A.K. Mal, Autonomous impact damage monitoring in a stiffened composite panel, *Journal of Intelligent Material Systems and Structures* 18 (2007) 623–633.
[19] J.W. Dally, W.F. Riley, *Experimental Stress Analysis*, third ed., Mcgraw-Hill College Division, 1991.
[20] E. Monaco, F. Franco, L. Lecce, Experimental and numerical activities on damage detection using magnetostrictive actuators and statistical analysis, *Journal of Intelligent Material Systems and Structures* 11 (2000) 567–578.
[21] Z. Chang, A.K. Mal, Wave propagation in a plate with defects, *Review of Progress in QNDE* 17 (1998) 121–128.
[22] D.J. Ewins, *Modal Testing, Theory, Practice, and Application*, second ed., Research Studies Pr, 2001.
[23] J.S. Bendat, A.G. Piersol, *Engineering Applications of Correlation and Spectral Analysis*, second ed., Wiley, New York, 1993.